PdPb-catalyzed decarboxylation of proline to pyrrolidine : highly selective formation of a biobased amine in water

PdPb catalyzed decarboxylation of proline to pyrrolidine: highly selective formation of a bio-based amine in water

Jasper Verduyckt,[a] Maarten Van Hoof,[a] Free De Schouwer,[a] Marike Wolberg,[a] Mert Kurttepeli,[b] Pierre Eloy,[c] Eric Gaigneaux,[c] Sara Bals,[b] Christine E. A. Kirschhock,[a] Dirk E. De Vos[a]*

[a] Centre for Surface Chemistry and Catalysis, Department of Microbial and Molecular Systems, KU Leuven - University of Leuven, Leuven Chem&Tech, Celestijnenlaan 200F, Post Box 2461, 3001 Heverlee, Belgium

[b] Electron Microscopy for Materials Science, UA - University of Antwerp, Groenenborgerlaan 171, 2020 Antwerp, Belgium

[c] Unité de Catalyse et Chimie des Matériaux Divisés, UCL – Université catholique de Louvain, Place L. Pasteur 1, 1348 Louvain-la Neuve, Belgium

KEYWORDS. PdPb, decarboxylation, L-proline, pyrrolidine, bio-based amine, water

ABSTRACT. Amino acids have huge potential as platform chemicals in the bio-based industry. Pd catalyzed decarboxylation is a very promising route for the valorization of these natural compounds derived from protein waste or fermentation. We report that the highly abundant and non-essential amino acid L-proline is very reactive in the Pd catalyzed decarboxylation. Full conversions are obtained with Pd/C and different Pd/MeO_x catalysts; this allowed to identify the

different side reactions and hence to map the reaction network. Due to the high reactivity of pyrrolidine, the selectivity for pyrrolidine was initially low. By carefully modifying Pd/ZrO_2 with Pb in a new, controlled manner – *i.e.* via two incipient wetness impregnation steps – the selectivity increased remarkably. Finally, a thorough investigation of the reaction parameters resulted in an increased activity of this new catalyst and an even further enhanced selectivity under a low H_2-pressure of 4 bar at 235°C in water. This ~~researcH~~ results in a very selective and sustainable production route for the highly interesting pyrrolidine.

Introduction

Amines are versatile building blocks for the synthesis of organic compounds, such as dyes, agrochemicals and pharmaceuticals.[1] Pyrrolidine is for example used in the synthesis of nicotine and rifamycin antibiotics.[2,3] Currently, this secondary amine is produced via the high temperature dehydration of 1,4-butanediol in the presence of ammonia using *e.g.* a ThO_2-Al_2O_3 catalyst at 300°C.[1] The diol on its turn is synthesized via oxidation of the fossil-based butane to maleic anhydride, which is subsequently hydrogenated to 1,4-butanediol in the DAVY process.[4] The different redox transformations render this route to pyrrolidine very inefficient. In this work we propose an alternative sustainable pathway for the synthesis of this important amine, starting from the amino acid L-proline as a renewable resource.

Amino acids can be produced in a green way via fermentation.[5,6] More importantly however, they will become increasingly available from protein rich waste streams.[7] Common agricultural waste fractions such as poultry feathers, dried distillers grains with solubles and press cakes from rapeseed, soybeans, algae, *etc*. contain up to 90% of proteins.[8] Sanders *et al.* predict that in this way more than 100 million tons of protein will be available if 10% of the fossil transportation fuel is replaced by biomass-derived fuels.[9] Work-up of these proteins includes extraction,

hydrolysis and subsequent separation of the amino acids. This final step still remains a big challenge, though new technologies based on electrodialysis and adsorption are emerging.[10–14]

Amino acids have huge potential as platform chemicals in the bio-based industry.[7] They can be catalytically converted to valuable nitriles via oxidative decarboxylation,[15–18] and to amino alcohols via hydrogenation.[19,20] Another very interesting class of valorization reactions is the direct decarboxylation to form amines. This reaction is *e.g.* catalyzed by enzymes or by α,β-unsaturated ketones that mimic the pyridoxal 5'-phosphate cofactor.[10,11,21] The use of enzymes suffers however from the need for an expensive cofactor in combination with a strict *pH* control and from a low volumetric productivity.[10,11,22] The use of homogeneous organocatalysts on the other hand suffers from the mandatory use of an organic solvent in combination with high catalyst loading and difficult catalyst recycling.[21] A viable alternative is the direct Pd catalyzed decarboxylation, which was first applied to the decarboxylation of fatty acids for the production of diesel-like compounds at 300°C.[23,24] Typically, the reaction is conducted with zerovalent Pd nanoparticles on a support. Recently, this technology was successfully adapted for the decarboxylation of itaconic acid to methacrylic acid and of (pyro)glutamic acid to 2-pyrrolidone in water at 250°C.[25,26] The extension of this technology to the production of amines from other amino acids has so far not been reported, obviously due to the instability of amines under these reaction conditions.

In this work the Pd catalyzed decarboxylation is successfully extended to the first highly selective formation of a bio-based amine in water, using L-proline as the substrate. An essential step to obtain high selectivities was the careful modification of the Pd catalyst with Pb via a new, controlled two-step incipient wetness approach.

Results & Discussion

Pd catalyst screening and unraveling the complex reaction network

In an initial screening different Pd catalysts were tested for the decarboxylation of L-proline (**1**) to pyrrolidine (**2**) with water as the solvent, using 4 mol% Pd at 6 bar N_2 and 225°C for 6 h (**Table 1**, entries 1-6). These reaction conditions were inspired by those recently reported by our group for the decarboxylation of pyroglutamic acid.[26] In general, L-proline (**1**) is very reactive for the decarboxylation, since almost all catalysts attain full conversion already at 225°C. The high conversions obtained with different catalysts allowed to identify the side products and hence to map the reaction network (**Scheme 1**). Due to its high reactivity, the selectivity to pyrrolidine (**2**) was initially low (2-33%). The first side route is the dehydrogenation of pyrrolidine (**2**) to form pyrrole (**3** - pathway **A**), which was observed especially for Pd/Al_2O_3 and Pd/ZrO_2. This reaction is known to be Pd catalyzed; group-IV metal oxide supports, like ZrO_2 and TiO_2, are known to favor the pyrrolidine dehydrogenation.[27] Pathway **B** leads to a plethora of side products, starting with a single dehydrogenation to form 1-pyrroline (**4**), which was identified using ^{1}H-NMR and GC-MS. This cyclic imine is hydrated to pyrrolidin-2-ol and its linear counterpart γ-aminobutyraldehyde. The cyclic amino alcohol is then again dehydrogenated to form 2-pyrrolidone (**5**). The latter is rather stable, but can be hydrolyzed to a minor extent, which consecutively opens the route to propionic acid (**9**).[26] The linear amino aldehyde is less stable and is most probably the origin of more side products, such as butyric acid (**10**), γ-hydroxybutyric acid (**11**) and γ-butyrolactone (**12**). The most important pathway **C** is initiated by the ring opening hydrogenolysis of pyrrolidine (**2**).[28] H_2 can be generated *in situ* in the water-gas shift reaction of CO formed in decarbonylation reactions (*cfr. infra*).[26] In this way *n*-butylamine (**6**) is formed, which is subsequently fully defunctionalized to propane (**7**) and

other volatile compounds. The presence of propane (**7**) was proven by performing gas phase Fourier transform infrared spectroscopy (FTIR) on the headspace of the reaction in entry 1 (**Table 1**). *n*-Butylamine (**6**) was merely observed in trace amounts, since it is highly reactive and readily defunctionalized to propane (**7**) and other volatiles. This was demonstrated with a reaction under the same conditions, starting from the linear amine: *n*-butylamine (**6**) was converted for 92% and only traces of products could be found in solution, while CO, CO_2, NH_3 and propane (**7**) were detected in the gas phase. The equilibrium between CO and CO_2 was clearly in favor of CO_2 (CO/CO_2 = 0.04); this confirms the occurrence of the water-gas shift reaction under these conditions. Finally, if L-proline (**1**) is not converted quickly enough, it gets the opportunity to react through a double intermolecular condensation; this gives rise to the diketopiperazine cyclodi-L-prolyl (**8**). This reaction represents most of the conversion in the blank reaction (**Table 1**, entry 13). The detailed identification of the observed compounds is given in the supporting information.

Table 1. Pd catalyst screening for the decarboxylation of L-proline to pyrrolidine.[a]

		Conversion	Selectivity [%]				
	Catalyst	[%]	Pyrrolidine	DKP [b]	Pathway A [c]	Pathway B [d]	Pathway C [e]
1	Pd/C	>99	2	<1	7	14	77
2	Pd/Al_2O_3	98	16	<1	25	16	43
3	$Pd/BaSO_4$	64	33	19	11	3	34
4	$Pd/CaCO_3$	>99	5	9	12	1	73
5	$Pd/MgAl_2O_4$	>99	6	<1	5	35	54
6	Pd/ZrO_2	>99	10	<1	27	17	46
7	$PdPb/CaCO_3$	64	41	23	2	5	29
8	$PdPb/MgAl_2O_4$	72	40	14	3	6	37
9	$PdPb/ZrO_2$ (A)	44	50	21	9	9	11
10	Pd/Al_2O_3 [f]	56	25	<1	29	5	41
11	Pd/ZrO_2 [f]	40	25	<1	32	10	33

12	PdPb/ZrO_2 (B)	45	67	11	2	20	<1
13	-	16	37	63	<1	<1	<1

[a] Reaction conditions: L-proline (0.2 mmol), 4 mol% Pd, water (2 mL), 225°C, 6 bar N_2, 6 h. [b] Cyclodi-L-prolyl, a diketopiperazine. [c] Side product from Pathway A is pyrrole. [d] 'Pathway B' represents 1-pyrroline, 2-pyrrolidone, propionic acid, butyric acid, γ-hydroxybutyric acid and γ-butyrolactone. [e] 'Pathway C' represents *n*-butylamine and mass loss from solution, resulting in the formation of propane and other volatiles. [f] 215°C.

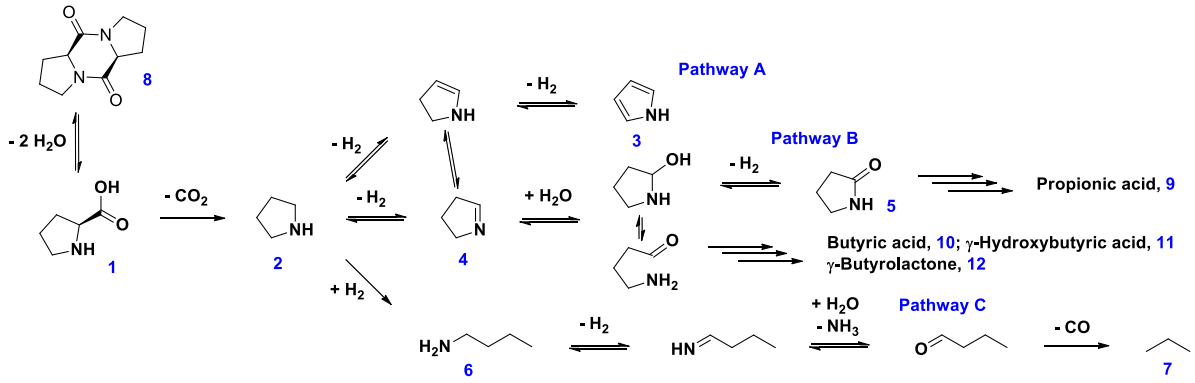

Scheme 1. Reaction network for the decarboxylation of L-proline. The detailed identification of the observed (numbered) compounds is given in the supporting information.

Modification with Pb

In search for a more selective catalyst to transform L-proline (**1**) into pyrrolidine (**2**), the modification of Pd with Pb was explored (**Table 1**, entries 7-9). Besides the commercially available PdPb/$CaCO_3$, also PdPb supported on a more acidic (ZrO_2) and a more basic ($MgAl_2O_4$) support were synthesized. The catalysts were prepared via a one-step impregnation with $(NH_3)_4PdCl_2$ together with $Pb(NO_3)_2$ according to Furukawa *et al.*,[29] followed by calcination and reduction. This clearly has a beneficial effect; the selectivity towards pyrrolidine (**2**) typically increases with more than 30%, irrespective of the support. PdPb/ZrO_2 (A), the most selective catalyst so far, already displays a pyrrolidine selectivity of 50% at 44% conversion. One might think that this increase is just due to a decrease in conversion. However, when

samples were analyzed at lower conversions using the conventional Pd catalysts, the selectivity never exceeded 25% (**Table 1**, entries 10-11). The selectivity increase is mainly due to the suppression of pathway **C**; ring opening hydrogenolysis of pyrrolidine (**2**), which opens the route towards propane (**7**), seems to be inhibited by the addition of Pb to Pd. Nevertheless, the latter reaction route is not completely blocked yet. This most likely results from the incomplete modification of Pd. Therefore the most selective catalyst was synthesized in a new, controlled manner to carefully modify all Pd sites. In this new method first Pd was distributed onto the ZrO_2 support by incipient wetness impregnation; subsequently the material was dried and calcined to remove the ligands. Afterwards, Pb was evenly deposited onto Pd by a second incipient wetness impregnation step. After a final drying, calcination and reduction step, PdPb/ZrO_2 (B) was obtained. For this newly synthesized catalyst the selectivity towards pyrrolidine (**2**) further increased up to 67% (**Table 1**, entry 12). Now the ring opening hydrogenolysis of pyrrolidine (**2**) is completely blocked, owing to the efficient modification of all Pd sites with Pb. In addition, Pb also significantly suppresses the dehydrogenation path towards pyrrole (**3**).

In order to prove that the higher selectivity of PdPb/ZrO_2 (B) compared to PdPb/ZrO_2 (A) is due to the better coverage of Pd with Pb, both catalysts were extensively characterized by high angle annular dark field – scanning transmission electron microscopy (HAADF-STEM) in combination with energy dispersive X-ray spectroscopy (EDX), by high resolution powder X-ray diffractometry (XRD) and by CO chemisorption. The particle size distribution of both samples was rather narrow with most of the nanoparticles situated between 4 and 8 nm (**Figure S1**). However, the high resolution X-ray diffractogram of the PdPb/ZrO_2 (A) sample shows unambiguous signals of a pure Pd phase (**Figure 1**). This clearly indicates that not all Pd is intimately mixed with Pb. Such signals are totally absent in the diffractogram of PdPb/ZrO_2 (B).

HAADF-STEM imaging accompanied with ~~the~~ EDX analysis was performed in order to determine the nature of the elements at the catalyst surface. **Figure 2** presents HAADF-STEM images (**Figure 2-(a) and -(g)**) and EDX elemental maps (**Figure 2-(b-e) and -(h-k)**) of both the PdPb/ZrO_2 (A) and PdPb/ZrO_2 (B) sample. The observed signals from Pd and Pb are visualized in red and green, respectively. By overlaying the EDX elemental maps of the Pd and Pb it is clear that for PdPb/ZrO_2 (A) the presence of Pd does not always correspond to the presence of Pb (**Figure 2-(f)**). However, for PdPb/ZrO_2 (B) the presence of Pd predominantly coincides with the presence of Pb (**Figure 2-(l)**). These measurements therefore confirm the hypothesis that Pd is much better covered by Pb in PdPb/ZrO_2 (B) than in PdPb/ZrO_2 (A). In addition, CO chemisorption experiments showed a lower apparent Pd dispersion for PdPb/ZrO_2 (B) compared to PdPb/ZrO_2 (A): 3% vs. 5% (**Table 2**). Since HAADF-STEM revealed very similar Pd particle size distributions for both catalysts, this difference is attributed to the better coverage of Pd by Pb in PdPb/ZrO_2 (B): when Pb is better covering the Pd surface, less CO is able to adsorb onto that surface. The same effect was observed in literature for CO chemisorption on Pd nanoparticles decorated or alloyed with Ga_2O_3, Sn, K, Mn and Cu.[30–32] Finally, X-ray photoelectron spectroscopy was performed to determine the electronic state of Pd and Pb in Pd/ZrO_2 and PdPb/ZrO_2 catalysts (**Table S1, Figure S2-3**). Pd was always in the metallic state, characterized by $3d_{5/2}$ emission peaks at 335.5 eV. This value corresponds very well with the 335.4 eV that was previously reported for Pd^0/ZrO_2.[33] Pb was in all catalysts present in both metallic and cationic states, as determined from $4f_{7/2}$ emission peaks at 136.6 and 138.8 eV, respectively. These values are in accordance with those reported for Pb^0 (137.1 eV) and PbO_2 (139.1 eV).[34] The presence of cationic Pb species might originate from exposure of the catalysts to air prior to the analysis; or it could mean that Pb was not fully reduced during the catalyst

synthesis. XPS did not give evidence for an influence of Pb on the electronic structure of Pd, this might however be attributed to the re-oxidation of Pb species prior to the analysis. Pd and Pb were used in the synthesis in a 3-to-1 molar ratio to produce the Pd_3Pb alloy that was proposed by Furukawa *et al*.[29] No evidence for this alloy was found in the XRD data, though this might be due to the much smaller nanoparticles formed in our synthesis, *viz.* 4-8 nm vs. 14-20 nm.

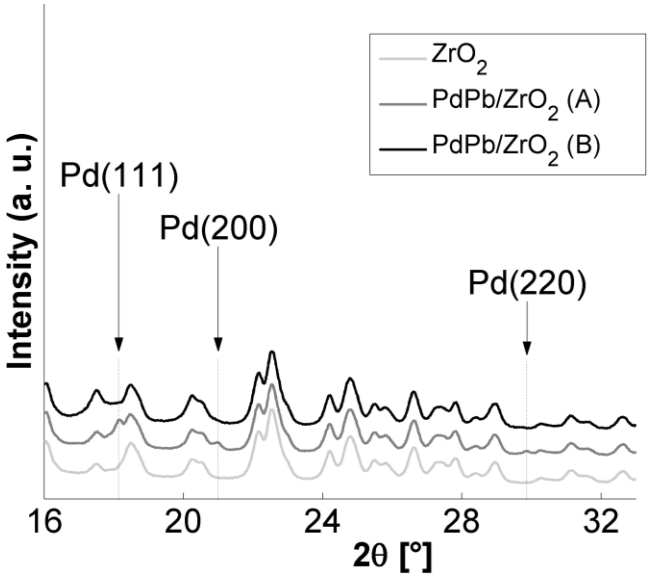

Figure 1. High resolution diffractograms of $PdPb/ZrO_2$ catalysts. The full pattern of Pd can be found in the supporting information (**Figure S4**).

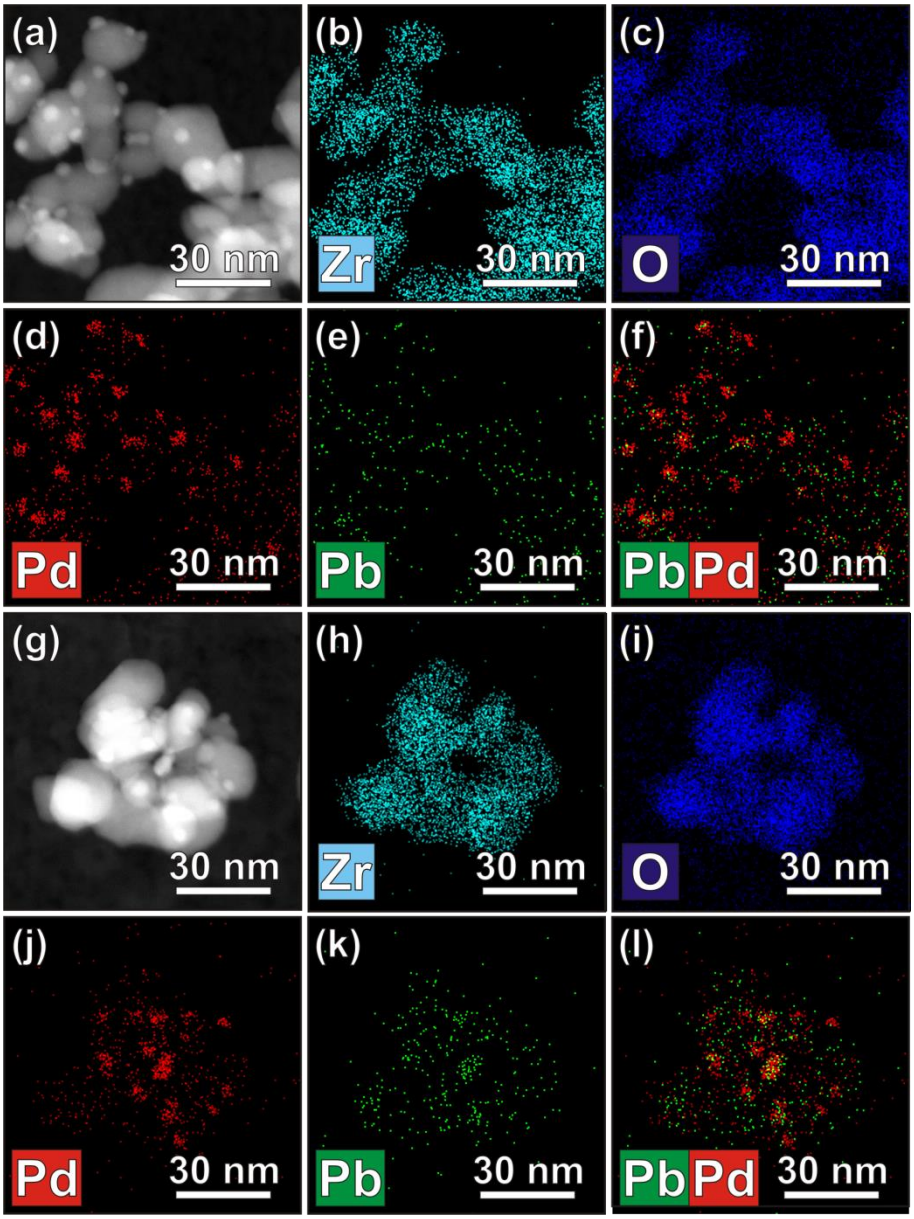

Figure 2. (a) & (g) HAADF-STEM images and (b-e) & (h-k) EDX elemental maps of $PdPb/ZrO_2$ (A) (top two rows) and $PdPb/ZrO_2$ (B) (bottom two rows). The overlap of the Pd and Pb signals can be studied from the mixed EDX elemental maps presented in (f) & (l).

Table 2. Pd dispersion of Pd/ZrO_2 and $PdPb/ZrO_2$ catalysts determined via CO chemisorption.

	Pd/ZrO_2	$PdPb/ZrO_2$ (A)	$PdPb/ZrO_2$ (B)
Pd dispersion [%]	8	5	3

Fine-tuning the reaction conditions

The modified $PdPb/ZrO_2$ (B) material is so far the best catalyst: it produces pyrrolidine (**2**) starting from L-proline (**1**) with a 67% selectivity, albeit at a rather low conversion of 45%. Nonetheless, side products from pathway **B**, as well as the diketopiperazine (**8**) are still formed. Further efforts are therefore devoted to increasing the rate of the catalytic reaction and to blocking the dehydrogenation that initiates pathway **B**.

Therefore first a temperature increase was investigated (**Table 3**). An increasing temperature leads to an increased conversion; at the optimum of 235°C the selectivity was not affected. However, at a temperature of 245°C ring opening hydrogenolysis of pyrrolidine (**2**) became prominent again, with a re-appearance of pathway **C** side products.

Table 3. Temperature optimization for the most selective catalyst.[a]

	Temperature [°C]	Conversion [%]	Selectivity [%]				
			Pyrrolidine	DKP [b]	Pathway A [c]	Pathway B [d]	Pathway C [e]
1	225	45	67	11	2	20	<1
2	235	52	69	6	4	21	<1
3	245	63	56	6	3	21	14

[a] Reaction conditions: L-proline (0.2 mmol), 4 mol% $PdPb/ZrO_2$ (B), water (2 mL), 6 bar N_2, 6 h. [b] Cyclodi-L-prolyl, a diketopiperazine. [c] Side product from Pathway A is pyrrole. [d] 'Pathway B' represents 1-pyrroline, 2-pyrrolidone, propionic acid and butyric acid. [e] 'Pathway C' represents mass loss from solution, resulting in the formation of propane and other volatiles.

Next, the addition of H_2 to the reaction atmosphere was explored (**Table 4**). A low H_2-pressure of 4 bar has a remarkably favorable influence on the activity of the $PdPb/ZrO_2$ (B) catalyst: a conversion of 88% is now reached within 6 h, with the decarboxylation as the dominant initial reaction (entries 1-2). Clearly, in this reducing atmosphere Pd more readily assumes its active zerovalent state.[35,36] In addition, the selectivity increases to 76%, largely owing to the inhibition

of the secondary dehydrogenation towards pyrrole (**3** - pathway **A**). When the H_2-pressure was increased to 10 bar, again ring opening hydrogenolysis became difficult to impede (entry 3). Further increase to 15 bar H_2 is even detrimental to the conversion level, either because H_2 occupies the active sites or because sintering of the metallic nanoparticles occurs (entry 4).

Table 4. Effect of varying partial pressures of H_2 in the reaction atmosphere.[a]

	P_{H2}	Conversion	Selectivity [%]				
	[bar]	[%]	Pyrrolidine	DKP [b]	Pathway A [c]	Pathway B [d]	Pathway C [e]
1	0[f]	52	69	6	4	21	<1
2	**4**	**88**	**76**	**4**	**1**	**19**	**<1**
3	10	88	64	2	1	9	24
4	15	27	41	44	<1	15	<1

[a] Reaction conditions: L-proline (0.2 mmol), 4 mol% $PdPb/ZrO_2$ (B), water (2 mL), 235°C, 2 bar N_2, 6 h. [b] Cyclodi-L-prolyl, a diketopiperazine. [c] Side product from Pathway A is pyrrole. [d] 'Pathway B' represents 1-pyrroline, 2-pyrrolidone, propionic acid and butyric acid. [e] 'Pathway C' represents mass loss from solution, resulting in the formation of propane and other volatiles. [f] 6 bar N_2.

Finally, **Table 5** studies the influence of the *pH* on the reaction, and especially its effect on pathway **B**, which is the only significant side route that subsists for the optimized reaction (**Table 4**, entry 2). The *pH* was adjusted using H_3PO_4 or NaOH; the natural *pH* of the starting solution at room temperature is 7. Both a more acidic and a more alkaline *pH* decrease the conversion. The alkaline environment induces a number of unidentified side reactions, decreasing the selectivity to pyrrolidine (**2**). On the other hand, the acidic environment results in a very high selectivity of 91% at 59% conversion, with a nearly total suppression of route **B**. The latter can be interpreted in two ways: i) in acidic conditions the dehydrogenation of pyrrolidine (**2**) to 1-pyrroline (**4**) occurs to a much lesser extent or ii) the decrease in conversion lowers the probability of consecutive side reactions. To verify which of those is the actual reason, a few

experiments were conducted as a function of time (**Table 5**, entries 4-5). When the reaction in the acidic environment was run at longer reaction times to increase the conversion, the selectivity drastically decreased again due to the formation of pathway **B** side products. Therefore the first explanation can be excluded; so the decrease in conversion is responsible for the very high selectivity. This was confirmed by decreasing the conversion of the reaction at neutral *pH* by decreasing the reaction time to 1 h: also in this way a selectivity of 95% was realized at a conversion of 58% (**Table 5**, entry 5).

Table 5. Effect of *pH* and reaction time.[a]

		Reaction	Conversion	Selectivity [%]				
	pH	time [h]	[%]	Pyrrolidine	DKP [b]	Pathway A [c]	Pathway B [d]	Pathway C [e]
1	2 [f]	6	59	91	5	2	2	<1
2	7	6	88	76	4	1	19	<1
3	12 [g]	6	67	34	<1	3	13	[h]
4	2 [f]	24	97	55	5	<1	40	<1
5	**7**	**1**	**58**	**95**	**<1**	**2**	**3**	**<1**

[a] Reaction conditions: L-proline (0.2 mmol), 4 mol% PdPb/ZrO_2 (B), water (2 mL), 235°C, 2 bar N_2 and 4 bar H_2. [b] Cyclodi-L-prolyl, a diketopiperazine. [c] Side product from Pathway A is pyrrole. [d] 'Pathway B' represents 1-pyrroline, 2-pyrrolidone, propionic acid, butyric acid, γ-hydroxybutyric acid and γ-butyrolactone. [e] 'Pathway C' represents mass loss from solution, resulting in the formation of propane and other volatiles. [f] *pH* was decreased by adding 0.4 eq. H_3PO_4. [g] *pH* was increased by adding 1 eq. NaOH. [h] Due to the complex product mixture the mass balance could not be determined accurately.

Mechanistic & kinetic insights

The new PdPb catalytic system for the decarboxylation of L-proline (**1**) to pyrrolidine (**2**) can now be run at very high selectivities, giving in only a little on the conversion level. The question remains why this modification with Pb results in a much higher selectivity than observed for the conventional Pd catalysts. Somorjai and co-workers investigated the formation of pyrrolidine (**2**)

by the hydrogenation of pyrrole (**3**) at room temperature on Pt.[28] In this case, the ring opening hydrogenolysis of pyrrolidine (**2**) to *n*-butylamine (**6**) could be avoided by lowering the desorption energy of pyrrolidine (**2**). This amine was shown to be surface-bound by the nitrogen atom. In addition, Furukawa *et al*. demonstrated that the modification of Pd with Pb renders Pd more electron rich.[29] Consequently, for the present reaction, Pd is expected to interact less strongly with the nitrogen atom of pyrrolidine (**2**), facilitating the desorption of the secondary amine. In this way consecutive side reactions on the Pd surface, such as ring opening hydrogenolysis can be avoided. In the same way pyrroline can desorb more easily from the Pd surface, avoiding the further dehydrogenation to pyrrole (**3**), but also potentially favoring the hydration to the amino alcohol and the amino aldehyde in pathway **B**. This switch is possible, since 1-pyrroline (**4**) and 2-pyrroline are in tautomeric equilibrium (**Scheme 1**).

To substantiate the reaction network that is proposed in ~~the first part of this work (~~**Scheme 1**~~)~~, the kinetic profiles of two reactions were recorded for the decarboxylation of L-proline (**1**) under the optimized reaction conditions. **Figure 3** depicts the kinetic profile obtained for the highly selective PdPb/ZrO_2 (B) catalyst. At the start of the reaction pyrrolidine (**2**) is produced very selectively. Pyrrole (**3**) and 1-pyrroline (**4**) quickly reach and maintain a low equilibrium concentration. After 1 h pyrrolidine (**2**) starts to convert into 2-pyrrolidone (**5**), which is clearly formed in a consecutive reaction. This leads to an optimal yield of pyrrolidine (**2**) of 69% at 86% conversion after 2 h. When the catalyst was recycled at this point, the conversion dropped due to an initial deactivation; however, the conversion in the subsequent runs stabilizes at 50-60% and the selectivity invariably remains very high, *i.e.* more than 90% (**Table S4**). **Figure 4** presents the kinetic profile of the reaction with Pd/ZrO_2. L-Proline (**1**) is decarboxylated very fast, therefore the first consecutive side reactions are already prominent in the early stages of the

reaction. The formation of pyrrole (**3**) is initially favored by Pd/ZrO_2; this product is however not stable under the applied reaction conditions. Pyrrole (**3**) is gradually hydrogenated back to pyrrolidine (**2**), which then reacts via one of the other two prominent pathways. The formation of propane (**7**, mass loss) therefore steadily increases from the start of the reaction. The concentration of 2-pyrrolidone (**5**) increases from the beginning as well, but reaches a plateau due to the subsequent formation of propionic acid (**9**).[26] Unlike propionic acid (**9**), butyric acid (**10**) is formed from the start of the reaction and is therefore unlikely to originate from 2-pyrrolidone (**5**). This product is believed to rather stem from γ-aminobutyraldehyde, which is in equilibrium with pyrrolidin-2-ol (**Scheme 1**).

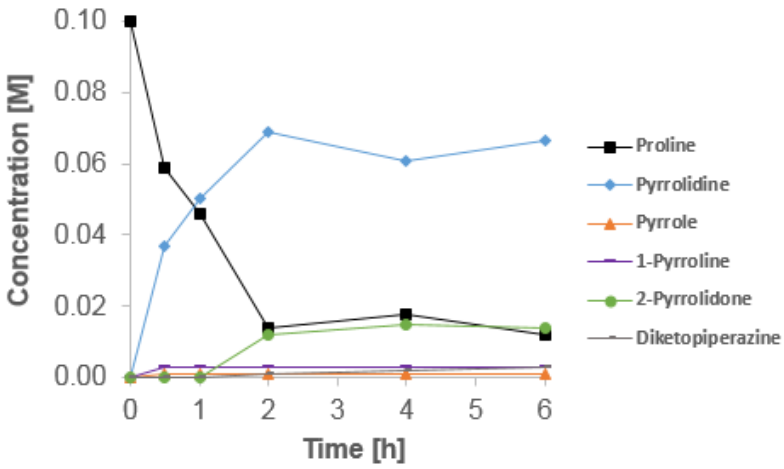

Figure 3. Time course of the decarboxylation of L-proline using $PdPb/ZrO_2$ (B). Reaction conditions: L-proline (0.2 mmol), 4 mol% $PdPb/ZrO_2$ (B), water (2 mL), 235°C, 2 bar N_2 and 4 bar H_2.

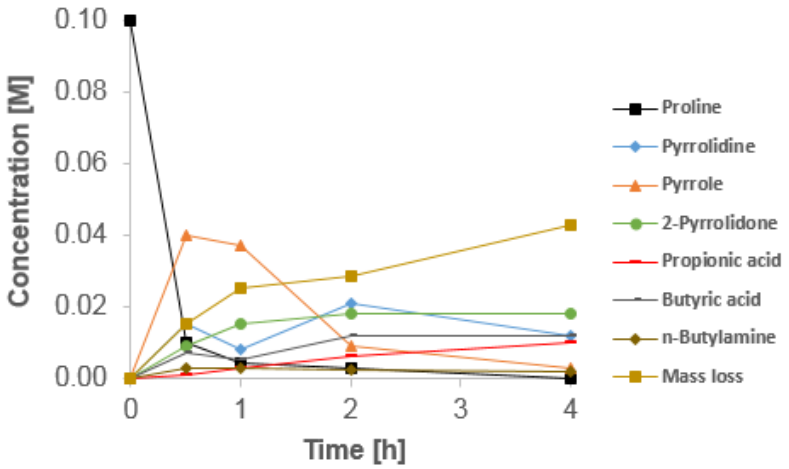

Figure 4. Time course of the decarboxylation of L-proline using Pd/ZrO_2. Reaction conditions: L-proline (0.2 mmol), 4 mol% Pd/ZrO_2, water (2 mL), 235°C, 2 bar N_2 and 4 bar H_2.

Finally, in order to confirm some of the hypotheses on consecutive transformation of the pyrrolidine product ~~once more~~, pyrrolidine itself was reacted for a short time (**Table 6**). Ring opening hydrogenolysis, which initiates pathway **C**, as well as the dehydrogenation to pyrrole (**3** - pathway **A**) are clearly impaired by the addition of Pb (entries 1, 3, 5). Moreover, the addition of H_2 further decreases the formation of pyrrole (**3** - pathway **A**) (entries 1-2, 5-6).

Table 6. Fate of pyrrolidine under the optimized reaction conditions.[a]

					Selectivity [%]		
	Catalyst	Pb	H_2	Conversion [%]	Pathway A [b]	Pathway B [c]	Pathway C [d]
1	$Pd/BaSO_4$	-	-	63	36	13	51
2	$Pd/BaSO_4$	-	x	35	6	34	60
3	Pd/ZrO_2	-	-	53	36	24	40
4	Pd/ZrO_2	-	x	56	38	21	41
5	$PdPb/ZrO_2$ (B)	x	-	50	8	64	28
6	$PdPb/ZrO_2$ (B)	x	x	58	5	53	42

[a] Reaction conditions: pyrrolidine (0.2 mmol), 4 mol% Pd, water (2 mL), 6 bar N_2 or 2 bar N_2 and 4 bar H_2, 235°C, 1 h or 20 min (for Pd/ZrO_2). [b] Side product from Pathway A is pyrrole.

[c] 'Pathway B' represents 1-pyrroline, 2-pyrrolidone, propionic acid and butyric acid. [d] 'Pathway C' represents *n*-butylamine and mass loss from solution, resulting in the formation of propane and other volatiles.

Conclusion

The Pd catalyzed decarboxylation has been successfully extended to the highly selective formation of a bio-based amine in water. During the initial screening of conventional Pd catalysts for the decarboxylation of the abundant and non-essential L-proline, pyrrolidine turned out to be very labile. The most important side reactions are initiated by either a dehydrogenation, leading to pyrrole, 1-pyrroline, 2-pyrrolidone, *etc.*, or by the ring opening hydrogenolysis of pyrrolidine to *n*-butylamine, which is further defunctionalized to propane and other volatiles. This led to very poor selectivities as low as 16% for Pd/Al_2O_3, the best catalyst reported for the decarboxylation of (pyro)glutamic acid to 2-pyrrolidone. Modifying the Pd catalysts with Pb was very favorable for the selectivity to pyrrolidine, owing to the blockage of the ring opening hydrogenolysis, as well as the partial inhibition of the dehydrogenation to pyrrole. The one-step impregnation of Pd together with Pb however resulted in an incomplete modification of Pd. Therefore a new, more controlled synthesis procedure based on a two-step incipient wetness approach was introduced. This procedure generated a $PdPb/ZrO_2$ catalyst in which Pd is always intimately mixed with Pb, as evidenced by HAADF-STEM in combination with EDX and by high resolution XRD. Careful exploration of the reaction parameters finally resulted in a very active and selective catalyst under a low H_2-pressure at 235°C in water. This new sustainable manufacture of pyrrolidine can be run either for 2 h with a high selectivity (80%) at high conversion (86%) or for only 1 h with a very high selectivity (95%) at somewhat lower conversion (58%).

Experimental section

Materials

All chemicals were used as received: L-proline (Sigma-Aldrich, >99%), pyrrolidine (Sigma-Aldrich, 99%), *n*-butylamine (Fischer Scientific, laboratory reagent grade), NaOH (Fischer Scientific, 99.1%), H_3PO_4 (Chem-Lab, 85% aq. solution), N_2 (Air Liquide, α1), H_2 (Air Liquide, N40), O_2 (Air Liquide, N25), He (Air Liquide, 99.9997%), CO (Air Liquide, 99.97%), Pd/C (5 wt%, Engelhard), $Pd/BaSO_4$ (5 wt%, Johnson Matthey), $Pd/CaCO_3$ (5 wt%, Johnson Matthey), $PdPb/CaCO_3$ (5 wt% Pd, 1 wt% Pb, Johnson Matthey), Al_2O_3 (Condea Chemie, Puralox NGa-150), $MgAl_2O_4$ (Sigma-Aldrich), ZrO_2 (Alfa Aesar), $(NH_3)_4PdCl_2.H_2O$ (Sigma-Aldrich, ≥99.99%), $Pb(NO_3)_2$ (Fluka, >98%), benzyl alcohol (Sigma-Aldrich, 99+%) and D_2O (Sigma-Aldrich, 99.9% D).

Catalyst synthesis

Conventional Pd catalysts (5 wt%) supported on Al_2O_3, $MgAl_2O_4$ and ZrO_2 were synthesized by incipient wetness impregnation according to De Schouwer *et al*.[26] In a typical procedure 1 g of support was impregnated with a solution of $(NH_3)_4PdCl_2$ in deionized water. Impregnated supports were then dried overnight at 60°C, granulated to particles with sizes between 250 and 500 µm, followed by calcination (35 min, 400°C, 2°C/min, 50 mL/min O_2) and reduction (1 h, 400°C, 2°C/min, 150 mL/min H_2). The synthesized catalysts were stored under N_2 until use.

$PdPb/ZrO_2$ (A) and $PdPb/MgAl_2O_4$ (5 wt% Pd, 3.27 wt% Pb) were synthesized by impregnation according to Furukawa *et al*.[29] First $(NH_3)_4PdCl_2$ and $Pb(NO_3)_2$ (Pd:Pb = 3:1 molar ratio) were dissolved in an aqueous solution (20 mL) by stirring the solution for 2 h at 75°C. 1 g of support material was then added; afterwards the stirred slurry was completely dried on the

stirring plate at 75°C. Next, the dried material was granulated to particles with sizes between 250 and 500 µm, calcined (35 min, 400°C, 2°C/min, 50 mL/min O_2) and subsequently reduced (1 h, 600°C, 2°C/min, 150 mL/min H_2). Finally, the catalysts were stored under N_2 until use.

$PdPb/ZrO_2$ (B) (5 wt% Pd, 3.27 wt% Pb) was synthesized by adapting the incipient wetness impregnation procedure from De Schouwer *et al.*[26] First, 1 g of ZrO_2 was impregnated with an aqueous solution of $(NH_3)_4PdCl_2$. After drying and calcining (35 min, 400°C, 2°C/min, air) the obtained material, it was impregnated with an aqueous solution of $Pb(NO_3)_2$ (Pd:Pb = 3:1 molar ratio). The doubly impregnated support was then dried overnight at 60°C, granulated to particles with sizes between 250 and 500 µm, followed by calcination (35 min, 400°C, 2°C/min, 50 mL/min O_2) and reduction (1 h, 600°C, 2°C/min, 150 mL/min H_2). Finally, the catalyst was stored under N_2 until use.

Catalyst characterization

XRD patterns were recorded with a Huber Guinier Camera G670 equipped with an image plate and utilizing Mo-$K\alpha_1$-radiation. TEM specimens were prepared by crushing the samples in powder form in an agate mortar and by suspending the resulting powder in ethanol. A drop of this suspension was deposited on a carbon coated TEM grid. HAADF-STEM images and EDX elemental maps were collected using an ~~aberration~~ corrected cubed FEI Titan operated at 200 kV, equipped with a Super-X detector for EDX analysis. SEM micrographs were recorded using a JEOL-6010LV SEM after depositing a Pd/Au layer on the samples using a JEOL JFC-1300 autofine coater under Ar plasma for 20 s. For CO chemisorption experiments 50 mg of the catalyst sample was loaded into a tubular reactor, ~~and~~ pretreated in a stream of 20 mL/min He at 130°C (heating rate: 10°C/min) for 1 h and ~~was~~ subsequently cooled to RT. For the titration of

the Pd surface, the He flow was reduced to 10 mL/min and pulses of 5 µL 100% CO were given with an interval of 2 min. The CO concentration in the outlet stream was followed with a Pfeiffer Omnistar quadrupole mass spectrometer. From the amount of CO adsorbed on the sample, a dispersion was calculated in the assumption that one CO molecule adsorbs per accessible Pd atom. N_2 physisorption measurements were performed using a Micromeritics 3Flex surface analyzer at -196°C. Before the measurements, the 100 mg samples were outgassed at 150°C for 6 h under vacuum. The XPS analyses were performed on a SSX 100/206 photoelectron spectrometer from Surface Science Instruments (USA) equipped with a monochromatized micro focused Al X-ray source (powered at 20 mA and 10 kV). The samples, powder pressed in small stainless steel troughs of 4 mm diameter, were placed on an insulating ceramic carousel. The pressure in the analysis chamber was around 10^{-6} Pa. The angle between the surface normal and the axis of the analyser lens was 55°. The analysed area was approximately 1.4 mm^2 and the pass energy was set at 50 eV. In these conditions, the full width at half maximum (FWHM) of the Au $4f_{7/2}$ peak of a clean gold standard sample was about 1.1 eV. A flood gun set at 8 eV and a Ni grid placed 3 mm above the sample surface were used for charge stabilisation. The following sequence of spectra was recorded: survey spectrum, C 1s, O 1s, Zr 3d, Zr 3p + Pd 3d, Pb 4f and C 1s again to check the stability of charge compensation with time. The C-(C,H) component of the C1s peak of carbon has been fixed to 284.8 eV to set the binding energy scale. Data treatment was performed with the CasaXPS program (Casa Software Ltd, UK); some spectra were decomposed with the least squares fitting routine provided by the software with a Gaussian/Lorentzian (85/15) product function and after subtraction of a non-linear baseline. Molar fractions were calculated using peak areas normalised on the basis of acquisition parameters and sensitivity factors provided by the manufacturer.

Catalytic reaction

In a typical reaction a solution of L-proline in deionized water (2 mL, 0.1 M) and a catalyst (4 mol% Pd) were loaded into a stainless steel reactor (11 mL). Next, the reactor was sealed and the atmosphere was flushed six times with N_2. Then, after pressurizing the reactor with 2 bar N_2 followed by 4 bar H_2, the mixture was magnetically stirred at 500 rpm and heated to 235°C. After 6 h the reaction was quenched by cooling with water and ice. Afterwards, the catalyst was separated from the solution by centrifugation. For recycling experiments the separated catalyst was washed three times with deionized water and dried overnight at 60°C. The catalyst was reused in a reaction of 2 h using the optimized conditions that are described in this paragraph. In each run, 5-10% of fresh catalyst was added to make up for the catalyst that was lost during the recycling.

Product analysis and identification

To determine the conversion of L-proline and the selectivities to the different products, the reaction mixtures were analyzed by ^{1}H-NMR. Samples were prepared by adding 300 µL of the reaction mixture to 300 µL of D_2O containing an external standard (benzyl alcohol, 0.1 M). ^{1}H-NMR spectra were recorded on a Bruker Ascend 400 MHz spectrometer equipped with a BBO 5 mm atma probe and a sample case. The broad signal of water was suppressed by applying an adapted zgpr pulse program: p1 9.75 µs; plw1 15W; plw9 5.7-05W; o1P on the resonance signal of water, determined and selected automatically. Besides ^{1}H-NMR, the products were also identified by gas chromatography coupled to mass spectrometry (GC-MS) with an Agilent 6890 GC, equipped with a HP-5ms column, coupled to a 5973 MSD mass spectrometer. The

identification of gaseous products was done using a Gasmet DX4000 FTIR gas analyzer. The IR data were processed with Calcmet Standard software version 12.161.

ASSOCIATED CONTENT

Supporting Information. Particle size distribution of PdPb/ZrO_2, XPS data, theoretical diffraction pattern of Pd, N_2 physisorption, mass transfer considerations, recycling experiments and product identification. This material is available free of charge via the Internet at http://pubs.acs.org.

AUTHOR INFORMATION

Corresponding Author

* E-mail: dirk.devos@kuleuven.be

Author Contributions

All authors have contributed to the work presented in this manuscript. J.V. and D.E.D.V. designed the experiments and prepared the manuscript. J.V. and F.D.S. performed catalyst synthesis. J.V. and M.V.H. carried out the decarboxylation experiments and did the product analysis. M.W. and C.E.A.K. performed XRD analysis and interpreted the results. M.K. and S.B. performed HAADF-STEM and EDX analysis and processed the results. P.E. and E.G. performed XPS analysis and processed the results. All authors have given approval to the final version of the manuscript.

Funding Sources

J.V. and F.D.S. thank FWO and IWT for doctoral fellowships. D.D.V. acknowledges IWT and FWO for research project funding. D.D.V. and C.E.A.K. acknowledge the Flemish government for long-term structural funding through Methusalem. D.D.V. and S.B. acknowledge Belspo (IAP-PAI 7/05) for financial support. S.B. is grateful for funding by the European Research Council (ERC starting grant #335078-COLOURATOMS). P.E. and E.G.: à compléter

Notes

The authors declare no competing financial interest.

ACKNOWLEDGMENT

J.V. and F.D.S. thank FWO and IWT for doctoral fellowships. D.D.V. acknowledges IWT for research project funding. D.D.V. and C.E.A.K. acknowledge the Flemish government for long-term structural funding through Methusalem. D.D.V. and S.B. acknowledge Belspo (IAP-PAI 7/05) for financial support. S.B. is grateful for funding by the European Research Council (ERC starting grant #335078-COLOURATOMS). P.E. and E.G.: à compléter The authors also thank the Department of Chemistry, University of Cologne, Germany for use of their XRD equipment. Finally, the assistance of Karel Duerinckx, Werner Wouters, Walter Vermandel, Ivo Stassen, Dries Jonckheere, Sabina Accardo and Bart Bueken with ^{1}H-NMR, pressure reactors, CO chemisorption, N_2 physisorption, SEM, gas phase FTIR and high throughput XRD, respectively, is very much appreciated.

ABBREVIATIONS

DKP, diketopiperazine.

REFERENCES

(1) Eller, K.; Henkes, E.; Rossbacher, R.; Höke, H. Amines, Aliphatic. *Ullmann's Encyclopedia of Industrial Chemistry,* sixth edition; Wiley-VCH Verlag: Weinheim, 2002; Vol. 2, pp 647–698.

(2) Malczewska-Jaskóła, K.; Jasiewicz, B.; Mrówczyńska, L. *Chem. Biol. Interact.* **2016,** *243,* 62–71.

(3) Bujnowski, K.; Synoradzki, L.; Zevaco, T.; Dinjus, E. Preparation of new rifamycin derivatives as antibacterial agents. Patent PL 220114 B1, Aug 31, 2015.

(4) Johnson Matthey. Butanediol & Co-Products. http://davyprotech.com/what-we-do/licensed-processes-and-core-technologies/licensed-processes/butanediol-thf-gbl/specification (accessed Mar 19, 2016).

(5) Breuer, M.; Ditrich, K.; Habicher, T.; Hauer, B.; Keβeler, M.; Stürmer, R.; Zelinski, T. *Angew. Chemie - Int. Ed.* **2004,** *43,* 788–824.

(6) Demain, A. L. *Ind. Biotechnol.* **2007,** *3,* 269–283.

(7) Tuck, C. O.; Perez, E.; Horvath, I. T.; Sheldon, R. A.; Poliakoff, M. *Science* **2012,** *337,* 695–699.

(8) Lammens, T. M.; Franssen, M. C. R.; Scott, E. L.; Sanders, J. P. M. *Biomass Bioenergy* **2012,** *44,* 168–181.

(9) Sanders, J.; Scott, E.; Weusthuis, R.; Mooibroek, H. *Macromol. Biosci.* **2007,** *7,* 105–117.

(10) Teng, Y.; Scott, E. L.; van Zeeland, A. N. T.; Sanders, J. P. M. *Green Chem.* **2011,** *13,* 624–630.

(11) Teng, Y.; Scott, E. L.; Witte-van Dijk, S. C. M.; Sanders, J. P. M. *N. Biotechnol.* **2015,** *33,* 171–178.

(12) Wang, B.; Li, O.; Zhang, Z.; Fan, Q.; Li, Z.; Wu, C.; Zhang, P.; Chen X. One kind of device system for joint production of amino acids and analogs thereof. Patent CN 204724028 U, Oct 28, 2015.

(13) Yuan, F.; Wang, Q.; Yang, P.; Tian, Y.; Cong, W. *Sep. Purif. Technol.* **2015,** *153,* 51–59.

(14) Lin, D.; Zhao, Q.; Yan, M. *J. Appl. Polym. Sci.* **2016,** *133,*43580.

(15) But, A.; Le Nôtre, J.; Scott, E. L.; Wever, R.; Sanders, J. P. M. *ChemSusChem* **2012,** *5,* 1199–1202.

(16) Matthessen, R.; Claes, L.; Fransaer, J.; Binnemans, K.; De Vos, D. E. *Eur. J. Org. Chem.* **2014,** 6649–6652.

(17) Claes, L.; Matthessen, R.; Rombouts, I.; Stassen, I.; De Baerdemaeker, T.; Depla, D.; Delcour, J. A.; Lagrain, B.; De Vos, D. E. *ChemSusChem* **2015,** *8,* 345–352.

(18) Claes, L.; Verduyckt, J.; Stassen, I.; Lagrain, B.; De Vos, D. E. *Chem. Commun.* **2015,** *51,* 6528–6531.

(19) Tamura, M.; Tamura, R.; Takeda, Y.; Nakagawa, Y.; Tomishige, K. *Chem. Commun.* **2014,** *50,* 6656–6659.

(20) Tamura, M.; Tamura, R.; Takeda, Y.; Nakagawa, Y.; Tomishige, K. *Chem.–Eur. J.* **2015,** *21,* 3097–3107.

(21) Lawson, A. Process for the production of amines. U.K. Patent 1008594-A, July 3, 1963.

(22) Dawes, G. J. S.; Scott, E. L.; Le Nôtre, J.; Sanders, J. P. M.; Bitter, J. H. *Green Chem.* **2015,** *17,* 3231–3250.

(23) Fu, J.; Lu, X.; Savage, P. E. *Energy Environ. Sci.* **2010,** *3,* 311–317.

(24) Snare, M.; Kubickova, I.; Maki-Arvela, P.; Eranen, K.; Murzin, D. Y. *Ind. Eng. Chem. Res.* **2006,** *45,* 5708–5715.

(25) Le Nôtre, J.; Witte-vanDijk, S. C. M.; van Haveren, J.; Scott, E. L.; Sanders, J. P. M. *ChemSusChem* **2014,** *7,* 2712–2720.

(26) De Schouwer, F.; Claes, L.; Claes, N.; Bals, S.; Degrève, J.; De Vos, D. E. *Green Chem.* **2015,** *17,* 2263–2270.

(27) Schäfer, M.; Böttcher, A.; Kramer, A.; Höhn, A.; Kaczmarek, R.; Henkes, E. Preparation of pyrrole and pyridine. U.S. Patent US 6,538,139 B1, Mar 25, 2003.

(28) Kliewer, C. J.; Bieri, M.; Somorjai, G. A. *J. Phys. Chem. C* **2008,** *112,* 11373–11378.

(29) Furukawa, S.; Suga, A.; Komatsu, T. *ACS Catal.* **2015,** *5,* 1214–1222.

(30) Ding, L.; Yi, H.; Zhang, W.; You, R.; Cao, T.; Yang, J.; Lu, J.; Huang, W. *ACS Catal.* **2016,** *6,* 3700–3707.

(31) Jbir, I.; Couble, J.; Khaddar-Zine, S.; Ksibi, Z.; Meunier, F.; Bianchi, D. *ACS Catal.* **2016,** *6,* 2545–2558.

(32) Shi, C.; Zhang, P. *Appl. Catal., B* **2012,** *115-116,* 190–200.

(33) Faticanti, M.; Cioffi, N.; De Rossi, S.; Ditaranto, N.; Porta, P.; Sabbatini, L.; Bleve-Zacheo, T. *Appl. catal., B* **2005,** *60,* 73–82.

(34) Hirano, T.; Kazahaya, Y.; Nakamura, A.; Miyao, T.; Naito, S. *Catal. Lett.* **2007,** *117,* 73–78.

(35) Lu, J.; Behtash, S.; Heyden, A. *J. Phys. Chem. C* **2012,** *116,* 14328–14341.

(36) Ahmadi, M.; Nambo, A.; Jasinski, J. B.; Ratnasamy, P.; Carreon, M. A. *Catal. Sci. Technol.* **2015,** *5,* 380–388.

For Table of Contents Only

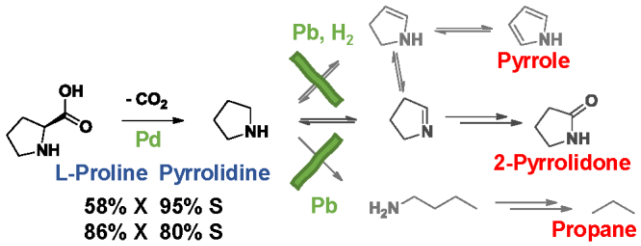

Supporting Information

PdPb catalyzed decarboxylation of proline to pyrrolidine: highly selective formation of a bio-based amine in water

Jasper Verduyckt,[a] Maarten Van Hoof,[a] Free De Schouwer,[a] Marike Wolberg,[a] Mert Kurttepeli,[b] Pierre Eloy,[c] Eric Gaigneaux,[c] Sara Bals,[b] Christine E. A. Kirschhock,[a] Dirk E. De Vos*[a]

[a] *Centre for Surface Chemistry and Catalysis, Department of Microbial and Molecular Systems, KU Leuven - University of Leuven, Leuven Chem&Tech, Celestijnenlaan 200F, Post Box 2461, 3001 Heverlee, Belgium*
[b] *Electron Microscopy for Materials Science, UA - University of Antwerp, Groenenborgerlaan 171, 2020 Antwerp, Belgium*
[c] *Unité de Catalyse et Chimie des Matériaux Divisés, UCL – Université catholique de Louvain, Place L. Pasteur 1, 1348 Louvain-la-Neuve, Belgium*

* E-mail: dirk.devos@kuleuven.be

1. Particle size distribution of $PdPb/ZrO_2$

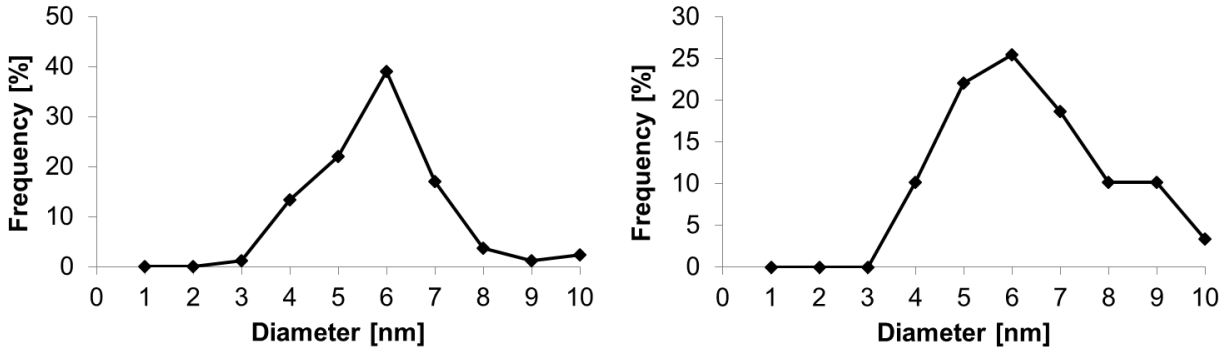

Figure S1. Particle size distribution of $PdPb/ZrO_2$ (A) (left) and $PdPb/ZrO_2$ (B) (right). The distribution was determined with 82 and 59 particles, respectively.

2. XPS data

Table S1. Summary of XPS data.

	Emission peak [eV]			Presence [%]		
	Pd $3d_{5/2}$	Pb $4f_{7/2}$		Pd $3d_{5/2}$	Pb $4f_{7/2}$	
Catalyst	Pd^0	Pb^0	Pb^{2+}	Pd^0	Pb^0	Pb^{2+}
Pd/ZrO_2	335.5	-	-	>99	-	-
$PdPb/ZrO_2$ (A)	335.5	136.6	138.8	>99	25	75
$PdPb/ZrO_2$ (B)	335.7	136.6	138.8	>99	20	80

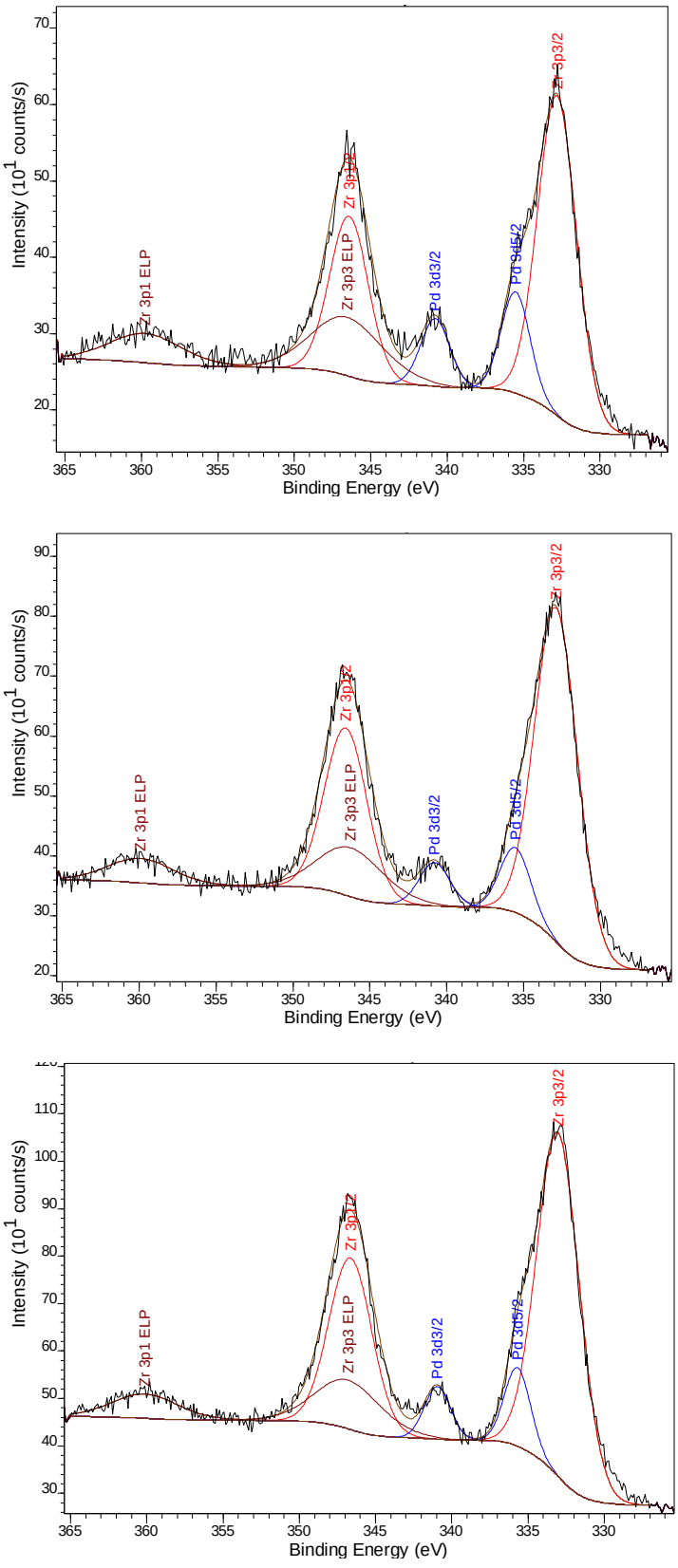

Figure S2. Pd 3d XPS of Pd/ZrO_2 (top), $PdPb/ZrO_2$ (A) (middle) and $PdPb/ZrO_2$ (B) (bottom).

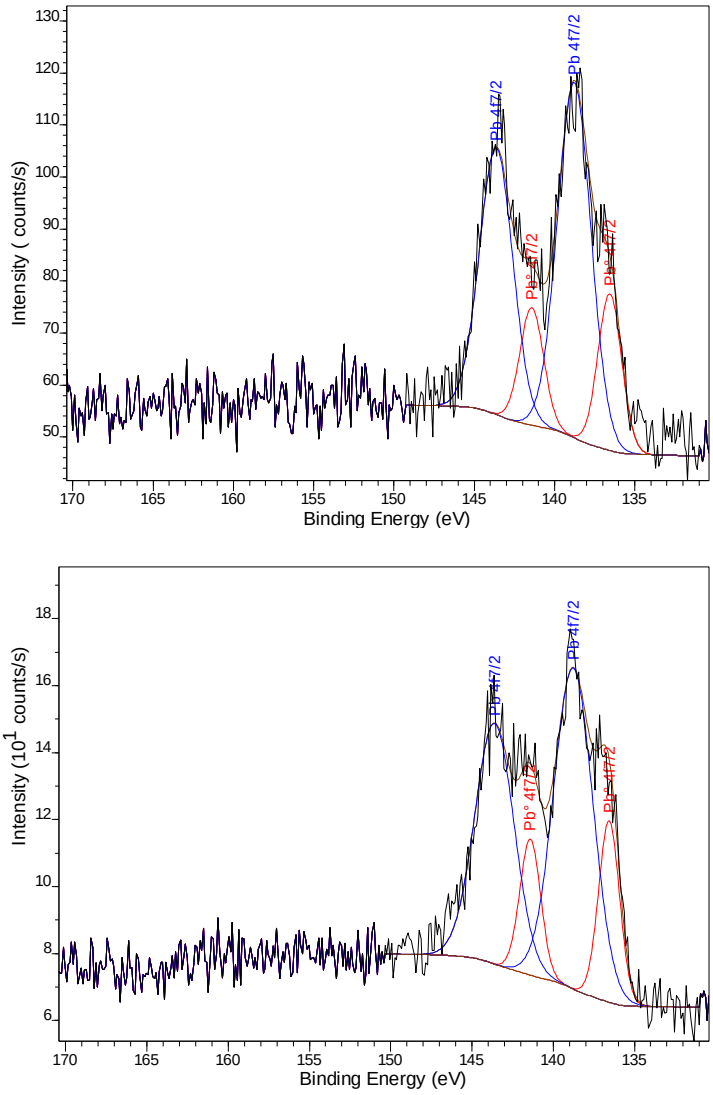

Figure S3. Pb 4f XPS of $PdPb/ZrO_2$ (A) (top) and $PdPb/ZrO_2$ (B) (bottom).

3. Diffractogram of Pd

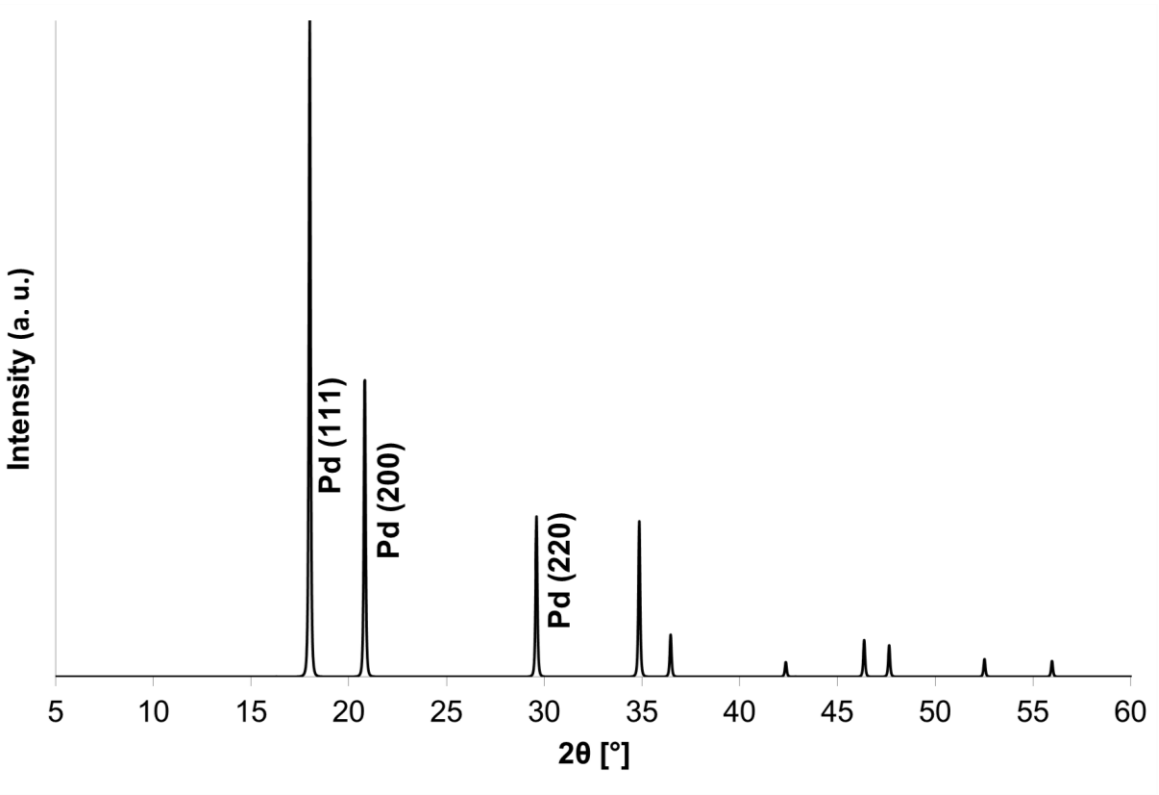

Figure S4. Theoretical X-ray diffraction pattern of Pd.[1]

4. N_2 physisorption

The textural properties of the $PdPb/ZrO_2$ catalysts were determined via N_2 physisorption measurements at -196°C (**Table S2, Figure S5**). The adsorption-desorption isotherms show type IV behavior according to the IUPAC classification and a hysteresis loop, which is typical for a mesoporous structure. $PdPb/ZrO_2$ (A), $PdPb/ZrO_2$ (B) and spent $PdPb/ZrO_2$ (B) have similar surface areas, pore volumes and pore size distributions.

Table S2. Textural properties of the $PdPb/ZrO_2$ catalysts obtained via N_2 physisorption.

Catalyst	S [m^2/g] [a]	V [cm^3/g] [b]	D [nm] [c]
$PdPb/ZrO_2$ (A)	41	0.20	16
$PdPb/ZrO_2$ (B)	42	0.18	13
$PdPb/ZrO_2$ (B) - spent	39	0.17	14

[a] BET surface area. [b] BJH pore volume derived from desorption isotherm. [c] BJH average pore diameter derived from desorption isotherm.

5. Mass transfer considerations

During the catalyst preparation the materials were granulated to particles with sizes between 250 and 500 µm. In the course of the reaction these granules break up in much smaller particles with sizes up to around 50 µm, as evidenced by scanning electron microscopy (SEM, **Figure S6**). Moreover, N_2 physisorption measurements showed that these particles are mesoporous (**Table S2, Figure S5**). Therefore mass transfer limitations are unlikely to occur. The absence of mass transfer issues was confirmed by increasing the stirring rate from 500 to 800 rpm for the optimized reaction (**Table S3**). A rotation speed of 800 rpm results in the same conversion (and selectivity) level as 500 rpm.

Table S3. Effect of stirring rate.[a]

	Rotation speed [rpm]	Conversion [%]	Selectivity [%]				
			Pyrrolidine	DKP [b]	Pathway A [c]	Pathway B [d]	Pathway C [e]
1	500	88	76	4	1	19	<1
2	800	89	80	5	<1	15	<1

[a] Reaction conditions: L-proline (0.2 mmol), 4 mol% $PdPb/ZrO_2$ (B), water (2 mL), 235°C, 2 bar N_2 and 4 bar H_2, 6 h. [b] Cyclodi-L-prolyl, a diketopiperazine. [c] Side product from Pathway A is pyrrole. [d] 'Pathway B' represents 1-pyrroline and 2-pyrrolidone. [e] 'Pathway C' represents mass loss from solution, resulting in the formation of propane and other volatiles.

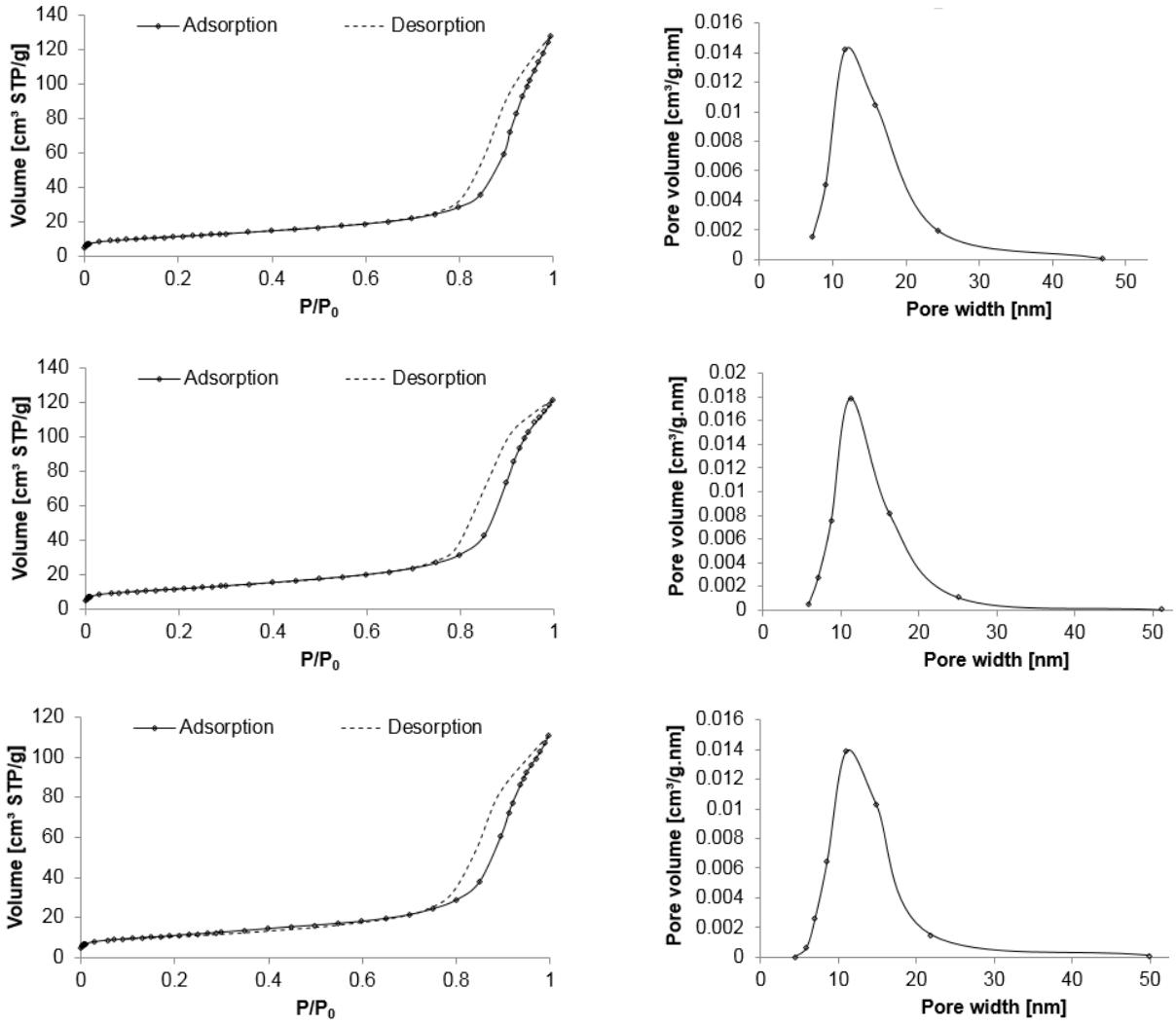

Figure S5. N_2 physisorption isotherms (left) and pore size distributions (right) of $PdPb/ZrO_2$ (A) (top), $PdPb/ZrO_2$ (B) (middle) and spent $PdPb/ZrO_2$ (B) (bottom). For the calculation of the pore size distribution the t-model of Harkins and Jura was used with Faas correction.

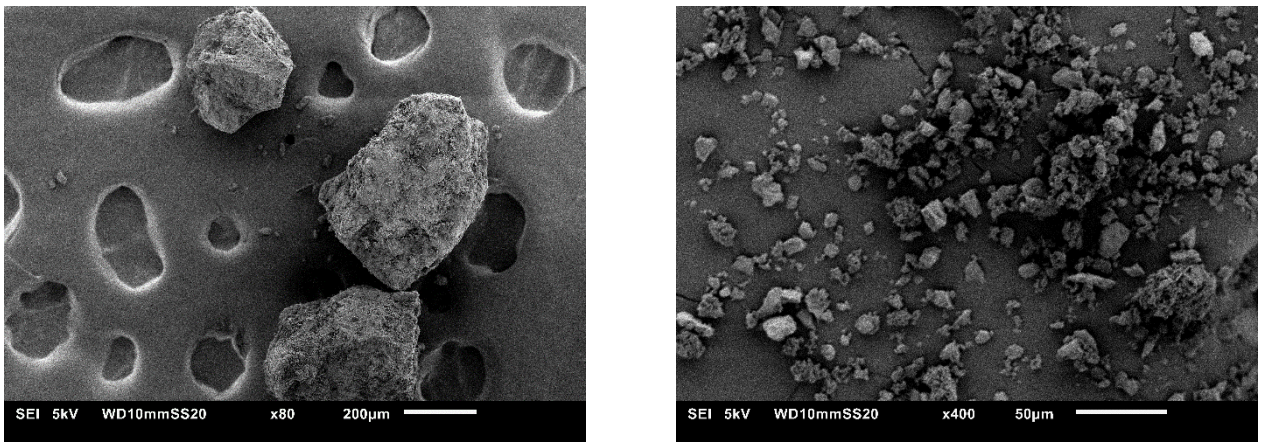

Figure S6. SEM micrographs of $PdPb/ZrO_2$ (B) before (left) and after (right) reaction.

6. Recycling experiments

Table S4. Recycling experiments.[a]

Run	Conversion [%]	Selectivity [%]				
		Pyrrolidine	DKP [b]	Pathway A [c]	Pathway B [d]	Pathway C [e]
1	86	80	1	1	18	<1
2	51	90	2	<1	8	<1
3	56	91	2	<1	7	<1

[a] Reaction conditions: L-proline (0.2 mmol), 4 mol% $PdPb/ZrO_2$ (B), water (2 mL), 235°C, 2 bar N_2 and 4 bar H_2, 2 h. [b] Cyclodi-L-prolyl, a diketopiperazine. [c] Side product from Pathway A is pyrrole. [d] 'Pathway B' represents 1-pyrroline and 2-pyrrolidone. [e] 'Pathway C' represents mass loss from solution, resulting in the formation of propane and other volatiles.

7. Product identification

General information: ^{1}H-NMR spectra were calibrated by setting the singlet signal of the external standard (benzyl alcohol) to 4.65 ppm.[2]

L-Proline (1, MW = 115 g/mol)

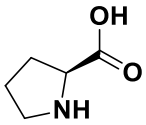

^{1}H-NMR (400 MHz, H_2O/D_2O): δ (ppm) = 3.98 (dd, 1H, -NH-C**H**-COOH), 3.37-3.30 (m, 1H, $-CH_2-C\mathbf{H}_2-NH-$), 3.24-3.16 (m, 1H, $-CH_2-C\mathbf{H}_2-NH-$), 2.34-2.22 (m, 1H, $-CH_2-C\mathbf{H}_2-CH<$), 2.04-1.89 (m, 3H, $-C\mathbf{H}_2-C\mathbf{H}_2-CH<$).

Pyrrolidine (2, MW = 71 g/mol)

^{1}H-NMR (400 MHz, H_2O/D_2O): δ (ppm) = 3.28 (t, 4H, $-CH_2-C\mathbf{H}_2-NH-$), 2.00 (t, 4H, $-C\mathbf{H}_2-CH_2-NH-$).
GC-MS (EI, 70 eV): m/z (rel. int., %): 71 (39), 70 (56), 68 (10), 43 (100), 42 (27), 41 (21), 40 (5), 39 (17).

Pyrrole (3, MW = 67 g/mol)

^{1}H-NMR (400 MHz, H_2O/D_2O): δ (ppm) = 6.92 (t, 2H, -CH=C**H**-NH-), 6.25 (t, 2H,-C**H**=CH-NH-).

GC-MS (EI, 70 eV): m/z (rel. int., %): 67 (100), 66 (9), 41 (28), 40 (21), 39 (36), 38 (17), 37 (11).

1-Pyrroline (4, MW = 69 g/mol)

^{1}H-NMR (400 MHz, H_2O/D_2O): δ (ppm) = 7.67 (s, 1H, -CH_2-C**H**=N-), 3.76 (t, 2H, -CH_2-C**H$_2$**-N=), 2.58 (t, 2H, -CH_2-C**H$_2$**-CH=N-), 1.82 (quint, 2H, -CH_2-C**H$_2$**-CH_2-).
GC-MS (EI, 70 eV): m/z (rel. int., %): 69 (68), 68 (56), 54 (5), 51 (5), 42 (32), 41 (100), 40 (22), 39 (35), 38 (16), 37 (6).

2-Pyrrolidone (5, MW = 85 g/mol)

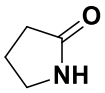

^{1}H-NMR (400 MHz, H_2O/D_2O): δ (ppm) = 3.42 (t, 2H, -CH_2-C**H$_2$**-NH-), 2.35 (t, 2H, -CH_2-C**H$_2$**-C(=O)-), 2.13 (quint, 2H, -CH_2-C**H$_2$**-CH_2-).
GC-MS (EI, 70 eV): m/z (rel. int., %): 85 (100), 84 (24), 56 (12), 42 (22), 41 (26), 40 (6), 39 (9).

***n*-Butylamine (6, MW = 73 g/mol)**

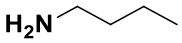

^{1}H-NMR (400 MHz, H_2O/D_2O): δ (ppm) = 2.99 (t, 2H, -CH_2-C**H$_2$**-NH_2), 1.64 (quint, 2H, -CH_2-C**H$_2$**-CH_2-), 1.39 (sx, 2H, -CH_2-C**H$_2$**-CH_3), 0.93 (t, 3H, -CH_2-C**H$_3$**).

Propane (7, MW = 44 g/mol)

Propane was identified along with CO, CO_2 and NH_3 using a Gasmet DX4000 FTIR gas analyzer and Calcmet Standard software version 12.161.

Cyclodi-L-prolyl, diketopiperazine (8, MW = 194 g/mol)

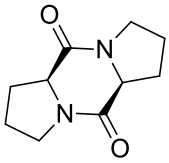

^{1}H-NMR (400 MHz, H_2O/D_2O): δ (ppm) = 4.40 (t, 2H, -NH-C**H**-COOH), 3.58-3.51 (m, 2H, -CH_2-C**H**$_2$-NH-), 3.48-3.39 (m, 2H, -CH_2-C**H**$_2$-NH-), 2.34-2.22 (m, 2H, -CH_2-C**H**$_2$-CH<), 2.04-1.89 (m, 6H, -C**H$_2$**-C**H**$_2$-CH<).
GC-MS (EI, 70 eV): m/z (rel. int., %): 194 (100), 166 (15), 139 (7), 138 (22), 137 (6), 124 (9), 111 (15), 110 (19), 97 (11), 96 (22), 83 (5), 70 (59), 69 (15), 68 (16), 55 (5), 42 (7), 41 (19), 39 (7).

Propionic acid (9, MW = 74 g/mol)

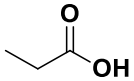

^{1}H-NMR (400 MHz, H_2O/D_2O): δ (ppm) = 2.19 (q, 2H, CH_3-C**H**$_2$-), 1.06 (t, 3H, C**H**$_3$-CH_2-).
GC-MS (EI, 70 eV): m/z (rel. int., %): 74 (100), 73 (63), 57 (38), 56 (19), 55 (24), 53 (5), 45 (53), 42 (10), 31 (5).

Butyric acid (10, MW = 88 g/mol)

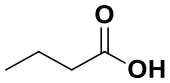

^{1}H-NMR (400 MHz, H_2O/D_2O): δ (ppm) = 2.16 (t, 2H, -CH_2-C**H**$_2$-COOH), 1.54 (sx, 2H, CH_3-C**H**$_2$-CH_2-), 0.90 (t, 3H, C**H**$_3$-CH_2-).
GC-MS (EI, 70 eV): m/z (rel. int., %): 88 (5), 73 (57), 71 (8), 60 (100), 55 (18), 45 (23), 43 (17), 42 (22), 41 (24), 39 (22), 38 (5).

γ-Hydroxybutyric acid (11, MW = 104 g/mol)

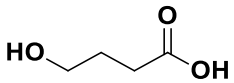

^{1}H-NMR (400 MHz, H_2O/D_2O): δ (ppm) = 3.48 (t, 2H, -CH_2-C**H**$_2$-OH), 2.43 (t, 2H, -CH_2-C**H**$_2$-COOH), 1.79 (quint, 2H, -CH_2-C**H**$_2$-CH_2-).

γ-Butyrolactone (12, MW = 86 g/mol)

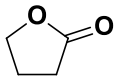

^{1}H-NMR (400 MHz, H_2O/D_2O): δ (ppm) = 4.44 (t, 2H, -CH_2-C**H**$_2$-O-), 2.58 (t, 2H, -CH_2-C**H**$_2$-C(=O)-), 2.37 (quint, 2H, -CH_2-C**H**$_2$-CH_2-).
GC-MS (EI, 70 eV): m/z (rel. int., %): 86 (52), 85 (14), 57 (6), 56 (31), 55 (6), 43 (6), 42 (100), 41 (64), 40 (18), 39 (24), 38 (8), 37 (5).

8. References

(1) Inorganic Crystal Structure Database, file 180871. Obtained from: Yan, X.; Lin, P.; Qi, X.; Yang, L. *Int. J. Mater. Res.* **2011,** *102,* 381-388.

(2) Babij, N. R.; McCusker, E. O.; Whiteker, G. T.; Canturk, B.; Choy, N.; Creemer, L. C.; De Amicis, C. V.; Hewlett, N. M.; Johnson, P. L.; Knobelsdorf, J. A.; Li, F.; Lorsbach, B. A.; Nugent, B. M.; Ryan, S. J.; Smith, M. R.; Yang, Q. *Org. Process Res. Dev.* **2016,** *20,* 661-667.